Bima Memoranda No. 14

A-PRIORI SELF-CALIBRATION

Melvyn Wright and Bob Sault

24-Oct-1990

ABSTRACT

We describe a method for calibrating aperture synthesis data automatically using a self-calibration algorithm with the a-priori positions and flux densities of the calibration sources. The algorithm adjusts the antenna gains to produce the best least squares fit to the theoretical instrumental point-spread function. These gains are then used to calibrate the source data. As an example of the use of the algorithm we present a map of the radio galaxy Cygnus A which was completely calibrated and mapped from a script command file.

INTRODUCTION

Aperture synthesis arrays now obtain data much faster than the astronomer is able to calibrate the data and produce a picture of the object of interest. It is not unusual for an astronomer to spend days or weeks reducing data which was obtained in hours. This has become a major discouragement for astronomers to use aperture synthesis instruments.

Aperture synthesis data is usually calibrated from observations of quasars interspersed with observations of the source(s) being mapped. The instrumental amplitude and phase response are then fitted to the quasar observations and removed from the source observations. This step often involves editing and weighting the calibrator data according to the signal-to-noise, and determining a flux density scale from a calibrator such as a planet observation. The source of interest is then mapped and the theoretical instrumental response deconvolved from the data to obtain an image of the brightness distribution.

The self-calibration algorithm has been successfully used to improve images by adjusting the antenna gains to be consistent with a model of the sky brightness obtained from a deconvolved image (e.g. Cornwell and Fomalont, 1989) Multichannel data are usually calibrated w.r.t. a wide bandwidth, "continuum" channel, or a strong line feature such as a maser. For many sources the signal is more evenly distributed between multiple line or continuum channels which all suffer from the same atmospheric fluctuations. If the relative gain of the channels is first removed from the data, then all the channels can be used to determine the antenna gains in an optimum way.

The self-calibration algorithm can also be used to obtain the a-priori gains from calibration sources. The process is equivalent to adaptive optics; the antenna gains are adjusted to produce the best fit to the theoretical instrumental response for the a-priori positions and flux densities of the calibration sources. The process is automatic and enables aperture synthesis data to be calibrated and mapped in close to real time.

In this memo we describe use of the MIRIAD self-calibration algorithm, using observations of the radio galaxy Cygnus A obtained with the BIMA millimeter array as an example.

OBSERVATIONS AND DATA REDUCTION

We used the BIMA 3-element millimeter array to map Cygnus A at 86 GHz. The data were obtained in a single 12-hour observation on 26 Feb 1990. The antennas were pointed in turn towards each of 3 fields centered on the central radio source and the hot spots in each radio lobe. Since the halfpower beamwidth of the 6m antennas is 2.3' at 86 GHz, we observed the radio emission from Cygnus A in 3 fields separated by 1'. The antennas were positioned along an east-west line with separations of 122 m. east, 0, and 73 m. west. The synthesised beamwidth is 2.28 x 3.06 arcsec. Because of the minimum antenna separation used, structure larger than 12 arcsec is not completely sampled, and the extended radio lobes are not represented in the maps presented. The data were calibrated

by observations of the Quasar 2005+403 at 30 min. intervals. Observations of 3C273 and Mars were also obtained to calibrate the flux density scale.

The calibration gains were determined by using the self-calibration procedure in the MIRIAD software package. The quasars have well determined positions and are unresolved at the interferometer baselines used. The theoretical response to the quasars is thus that of a point source at the phase center with an amplitude equal to the flux density of the quasar. The flux densities were interpolated from a table of flux density versus time and frequency which were calibrated from planet observations. Interferometer observations of planets or other resolved sources can also be used in the self calibration procedure if an accurate model is available. For planet observations on short baselines we use a disk model with axes obtained from the ephemeris, and surface brightness given by Ulich (1981). The self calibration procedure makes a simultaneous least squares fit to the calibration observations. This procedure is equivalent to the customary fitting of amplitudes and phases to the calibrator data, but with the advantages that the data are properly weighted according to the signal to noise ratio, and that phase closure, and 2pi phase ambiguities are automatically handled. We used a time interval of 45 minutes for the calculation of the antenna gains from the calibrator data.

Figure 1 and 2 show amplitude and phase of the calibrator before and after the a-priori calibration. Figure 3 shows the antenna gains. The procedure has correctly handled the phase and gain jump when antenna 2 was re-focussed. Figure 4 shows the synthesised map of the calibrator, 2005+403, and the difference from the theoretical point-spread function scaled to the amplitude of the calibrator. The rms difference is 4% of the peak, which is close to the theoretical noise level for the integration time on the calibrator.

The gains derived from the calibrator were applied to the observations of Cygnus A. The 3 fields of Cygnus A were then cleaned using the Hogbom algorithm, and combined using a linear mosaicing algorithm. This combination process corrects for primary beam attenuation, and weights pixels so as to minimize the mean square error in the resultant map (i.e. the combination is optimum in the Weiner sense). The restored map is shown in Figure 5a. The central radio source and hot spots are clearly evident on this map. Since the instrumental phase stability, and weather were quite good, the a-priori calibration gives an rms noise level of 50 mJy, only twice that calculated from the receiver noise, bandwidth, and integration time. These results were checked with a more conventional calibration procedure.

The rms noise level was further reduced by using this (mosaiced) map as a model for self-calibration in order to remove atmospheric phase fluctuations on time scales shorter than the calibration interval. The time scale for the self-calibration was set to 5 minutes, so that the observation of all 3 fields (each sampled at 150 s. intervals) could be used to determine the antenna gains

The self-calibration algorithm performs a least squares fit by minimizing

$$\mathrm{Sum}\{\ [|gi*\mathrm{conj}g(gj)\ V' - V|/\mathrm{sigma}]^{**}2\}$$

Here gi, gj are the unknown antenna gains, V' is the observed source visibility, and V is the visibility computed from the model. Sigma is the noise estimated from the system temperature, bandwidth, and integration time. The antenna gains are assumed to be independent of the pointing center and the frequency channel. Thus the summation can be taken over all the observed fields, and all frequency channels. In the case of the Cygnus A observations, the data comprises of 3 fields, and 2 frequency channels (the upper and lower sideband of the first local oscillator).

In order to use the mosaiced image as the model for the self-calibration, we first weight the model by the primary beam centered at the various pointing centers, and then use these multiple models in a simultaneous least squares solution for the antenna gains.

The resultant corrected visibilities were then remapped, cleaned and mosaiced.

The restored image is given in Figure 5b. This image shows a factor of 2 improvement in dynamic range. This whole reduction procedure was driven by a script written in csh which passes control to each of a series of MIRIAD tasks to calibrate, map, deconvolve, mosaic and plot the images. The script is easily modified to handle different situations.

RESULTS

The positions of the source components were measured from the mosaiced image with only a-priori calibration, and are thus measured with respect the the assumed position for 2005+403 (RA(1950)=20:05:59.56 DEC=40:21:01.80). Since 2005+403 is quite close to Cygnus A, phase errors due to errors in the assumed baseline are very small. At 86 GHz, a baseline error, dB nanosecs, leads to a phase error, 360 x 86 x dB.ds degrees, where ds is the angle between source and calibrator. The baseline was determined in the usual way from observations of quasars with well determined positions. The error in the baseline, $dB \sim 0.001$ in each coordinate, so that the phase error due to baseline error ~ 0.5 degrees, much smaller than the atmospheric phase fluctuations of 5 - 10 degrees. The positions are good to about 0.1 of the synthesised beamwidth.

Table 1: Positions and flux densities for Cygnus A components.

component	RA	DEC	Flux density	Size
A	19 57 38.97 (.03)	40 36 09.6 (.3)	2.17	
B	19 57 39.15 (.05)	40 36 05.1 (.5)	0.4	
Center	19 57 44.45 (.03)	40 35 46.1 (.3)	0.85	
D	19 57 49.11 (.03)	40 35 24.8 (.3)	4.2 (0.4)	

The positions are in excellent agreement with those given by Dreher (1981) at 22 GHz. The position for component B refers to the separate peak seen in Figure 5a. Component B is much better defined than in the maps presented by Wright and Birkinshaw (1984), and the position given here is to be preferred.

The flux densities are also measured from the restored image (Figure 5a). The flux densities on the self-calibrated image (Figure 5b) are about 10% higher. The flux densities given in Table 1 are the integrated fluxes within each source component, including the more diffuse emission surrounding the peaks. We attributed 0.4 Jy to component B, out of a total 2.57 for the A/B component complex.

CONCLUSIONS

Aperture synthesis data can be calibrated using a self-calibration algorithm and the a-priori positions and flux densities of the calibration sources. The process is automatic and enables aperture synthesis data to be calibrated and mapped in close to real time.

For the multiple field observations of Cygnus A, the calibration and imaging techniques used in the MIRIAD software have given a higher dynamic range image with a single 12 hour observation, than obtained with 10 baselines used in the previous observations with the same instrument.

FIGURES

1. Amplitude and phase of the calibrator before a-priori calibration. The amplitude is in units of Ta* (K).
2. Amplitude and phase of the calibrator after a-priori calibration. The amplitude is now calibrated flux density in units of Jy.
3. The antenna gains for a 45-minute averaging interval. The amplitude is in units of SQRT(Jy/K) for each antenna.
4. (a) Synthesised map of the calibrator. Contour interval 0.1 Jy/beam.
   (b) The difference between the map of the calibrator and the beam scaled to the amplitude of the calibrator. Contours at .05 .1 .2 Jy/beam.
5. (a) Mosaic Map of Cygnus A after deconvolution. (b) after selfcalibration. Contours at .05 .1 .2 .4 .6 .8 Jy/beam.

REFERENCES

Cornwell, T. and Fomalont, E.B., 1989, Synthesis Imaging in Radio Astronomy. ASP conf. series, 6, 185

Dreher, J.W., 1981, A.J. 86, 833

Ulich, B.L.,1981, A.J., 86, 1619.

Wright, M.C.H., and Birkinshaw, M., 1984, Ap.J. 281, 135.

all caluv 86.2020 GHz 1– 2

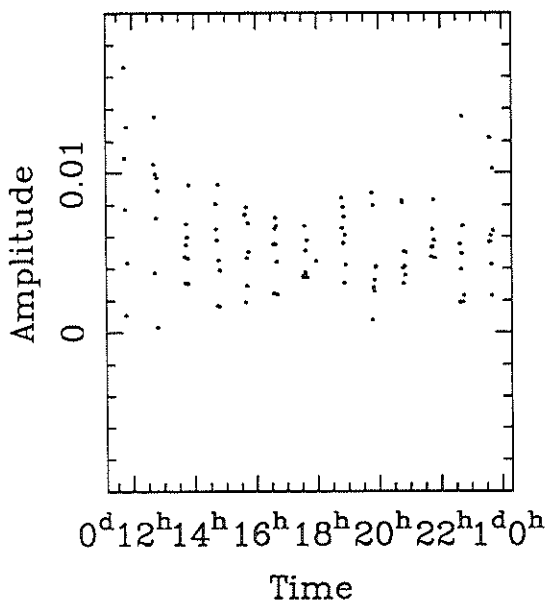

all caluv 86.2020 GHz 2– 3

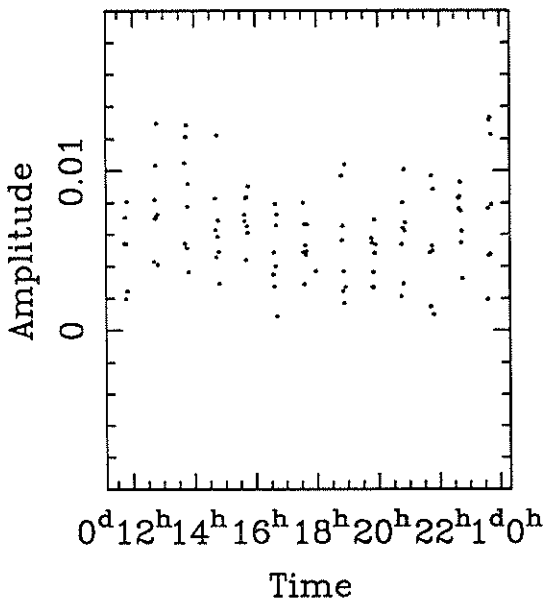

all caluv 86.2020 GHz 1– 3

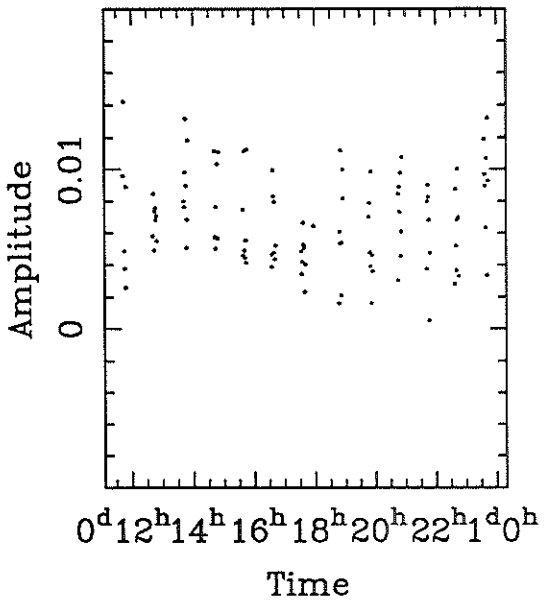

all caluv 86.2020 GHz 1– 2

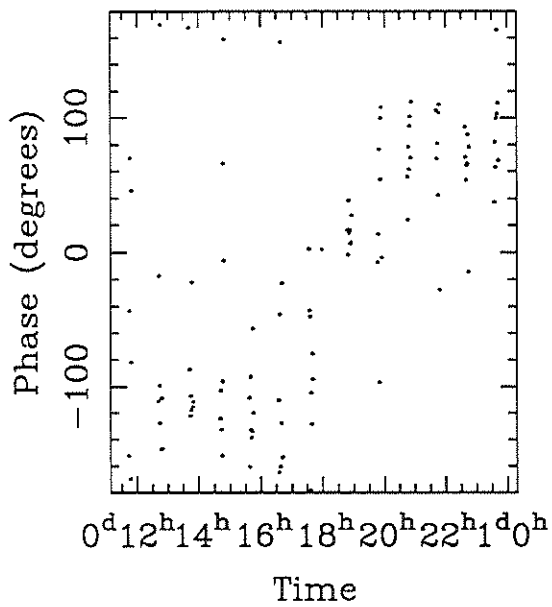

all caluv 86.2020 GHz 2– 3

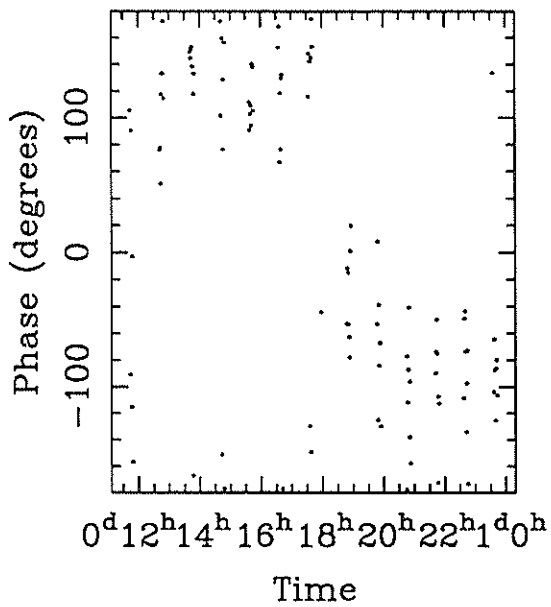

all caluv 86.2020 GHz 1– 3

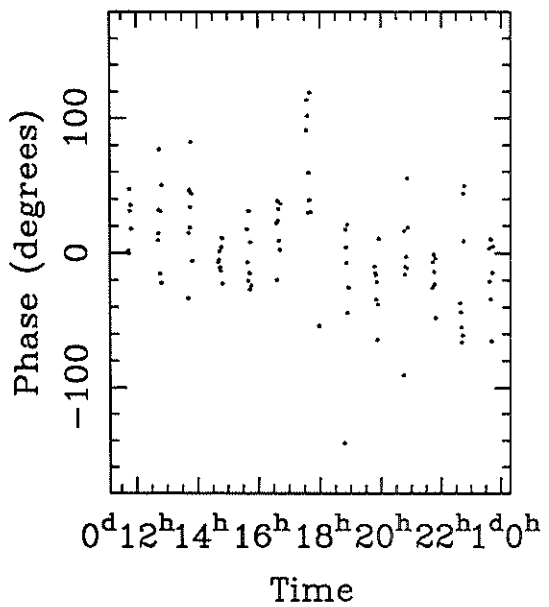

all caluv 86.2020 GHz 1– 2

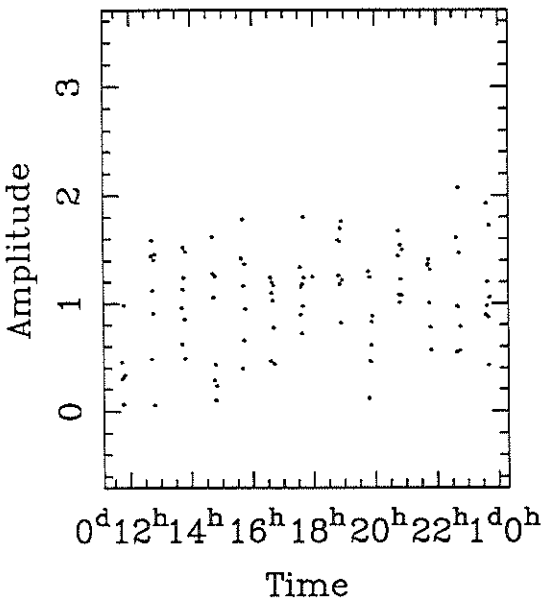

all caluv 86.2020 GHz 2– 3

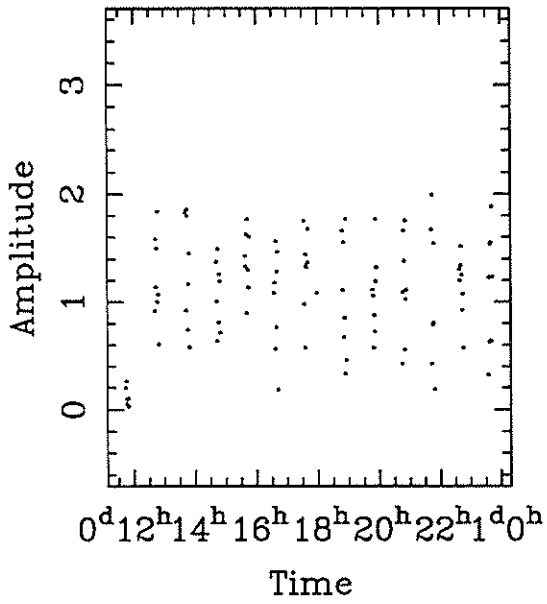

all caluv 86.2020 GHz 1– 3

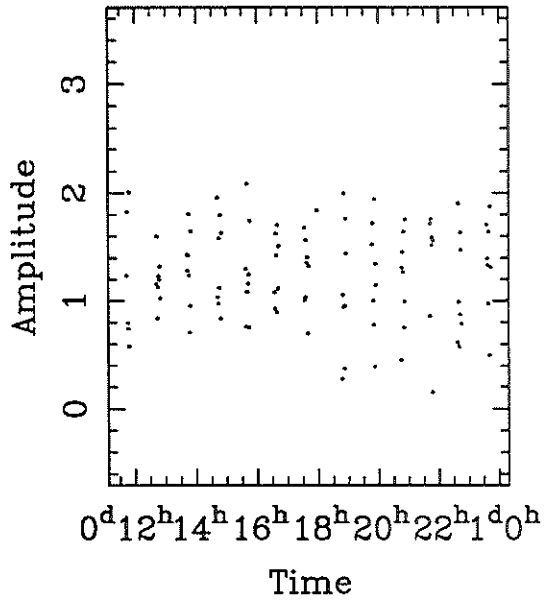

all caluv 86.2020 GHz 1– 2

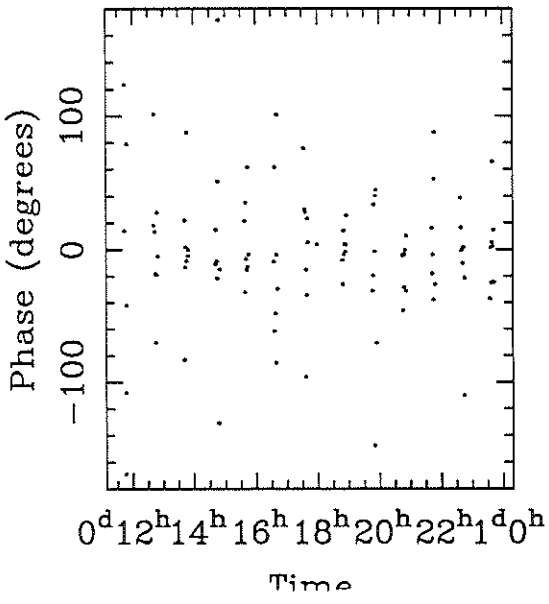

all caluv 86.2020 GHz 2– 3

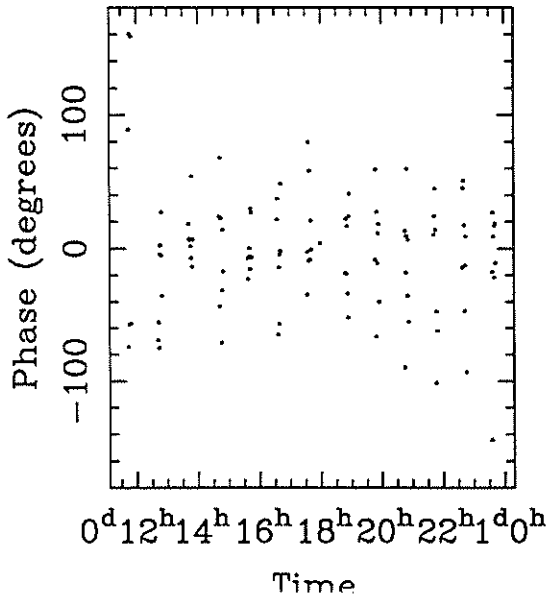

all caluv 86.2020 GHz 1– 3

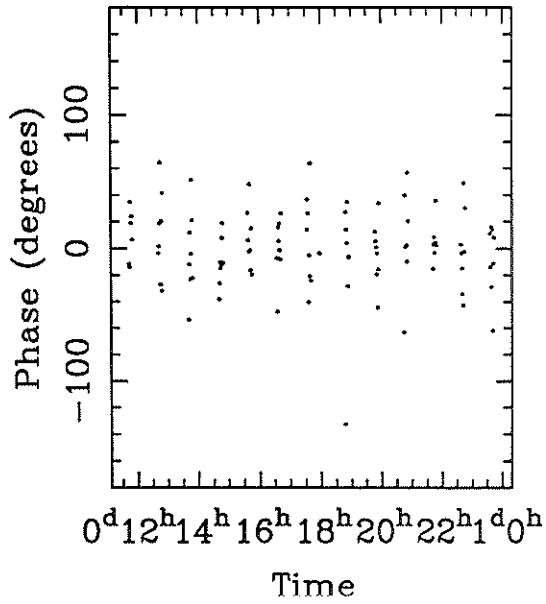

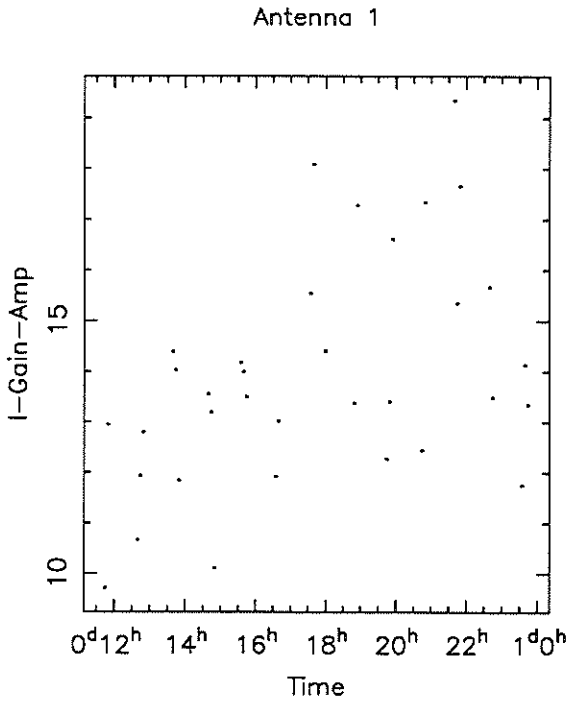
Antenna 1
I-Gain-Amp
10
15
0d12h 14h 16h 18h 20h 22h 1d0h
Time

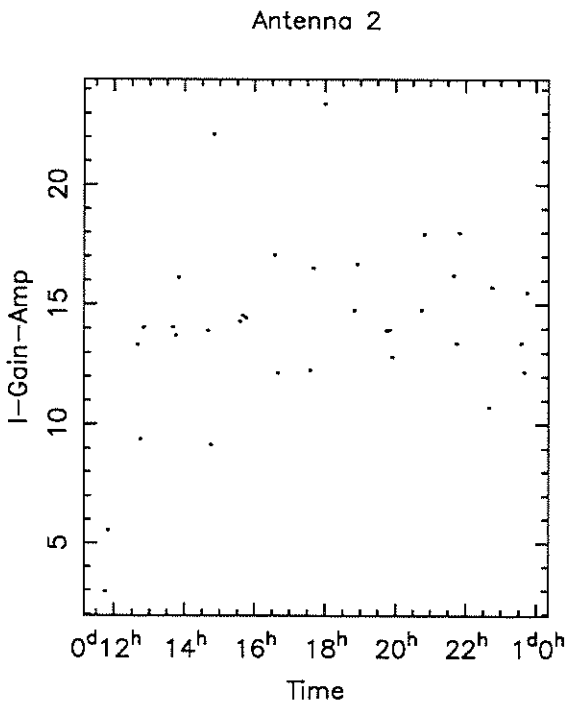
Antenna 2
I-Gain-Amp
5
10
15
20
0d12h 14h 16h 18h 20h 22h 1d0h
Time

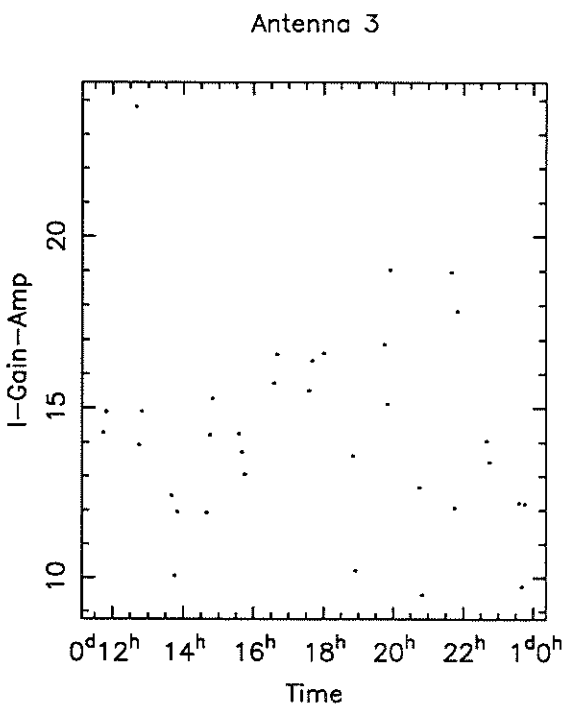
Antenna 3
I-Gain-Amp
10
15
20
0d12h 14h 16h 18h 20h 22h 1d0h
Time

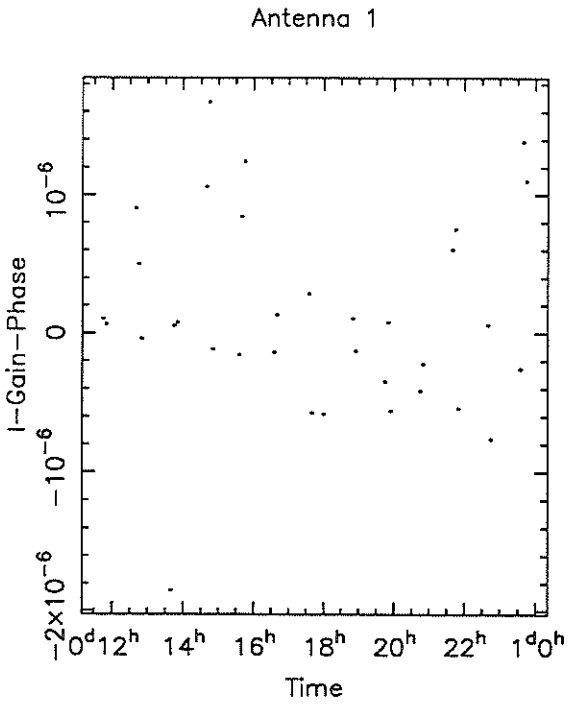
Antenna 1
I-Gain-Phase
-2x10-6
-10-6
0
10-6
0d12h 14h 16h 18h 20h 22h 1d0h
Time

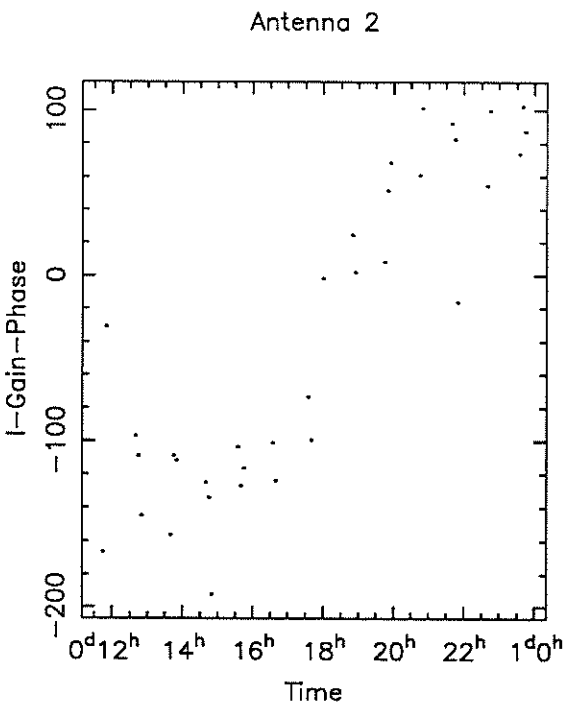
Antenna 2
I-Gain-Phase
-200
-100
0
100
0d12h 14h 16h 18h 20h 22h 1d0h
Time

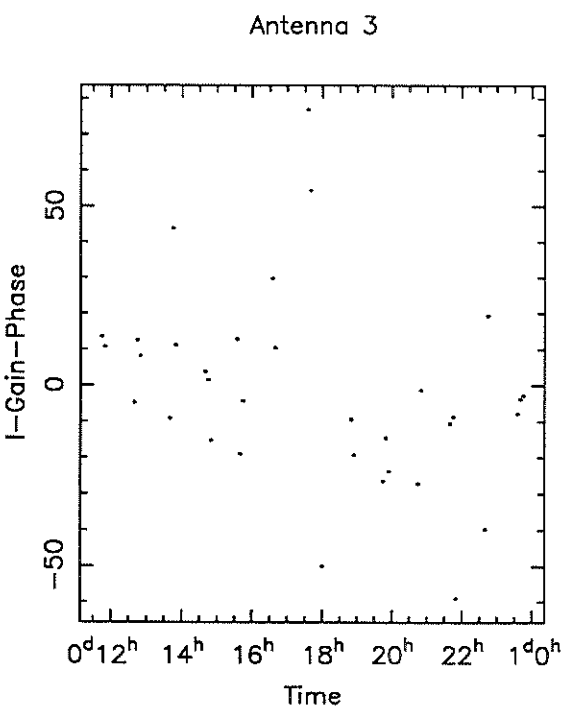
Antenna 3
I-Gain-Phase
-50
0
50
0d12h 14h 16h 18h 20h 22h 1d0h
Time

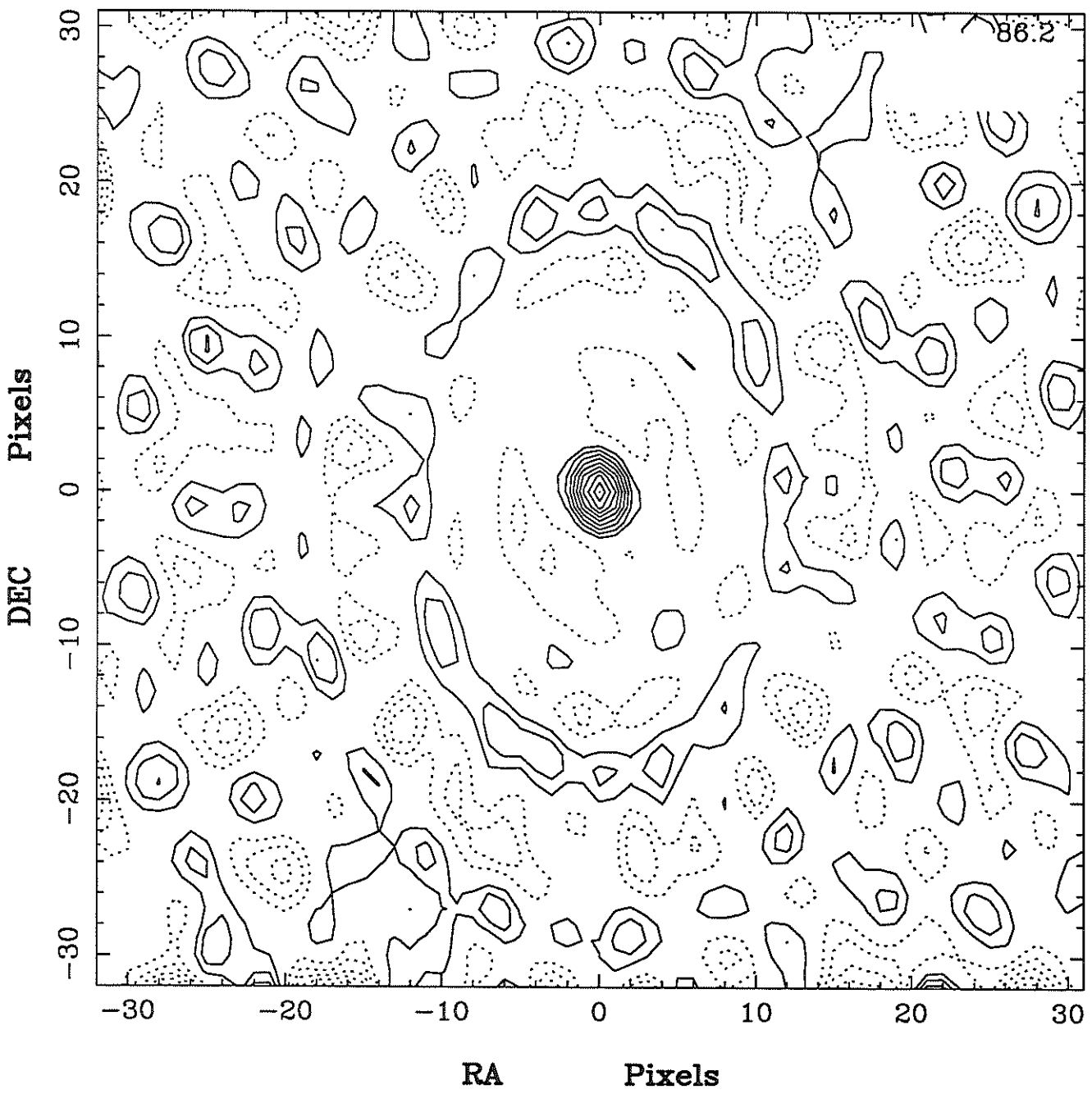

2005P403

20:05:59.56 40:21:01.80

File: map
Freq: 0.000000 (GHz)
Crval3: 86.2020 GHz
Max: 0.992781
Min: −0.582612
Units: JY/BEAM

Axes: 64 x 64 x 1
−1.00 x 1.00 x 0.31

Contours: 10

0.099	0.199
0.298	0.397
0.496	0.596
0.695	0.794
0.894	0.993

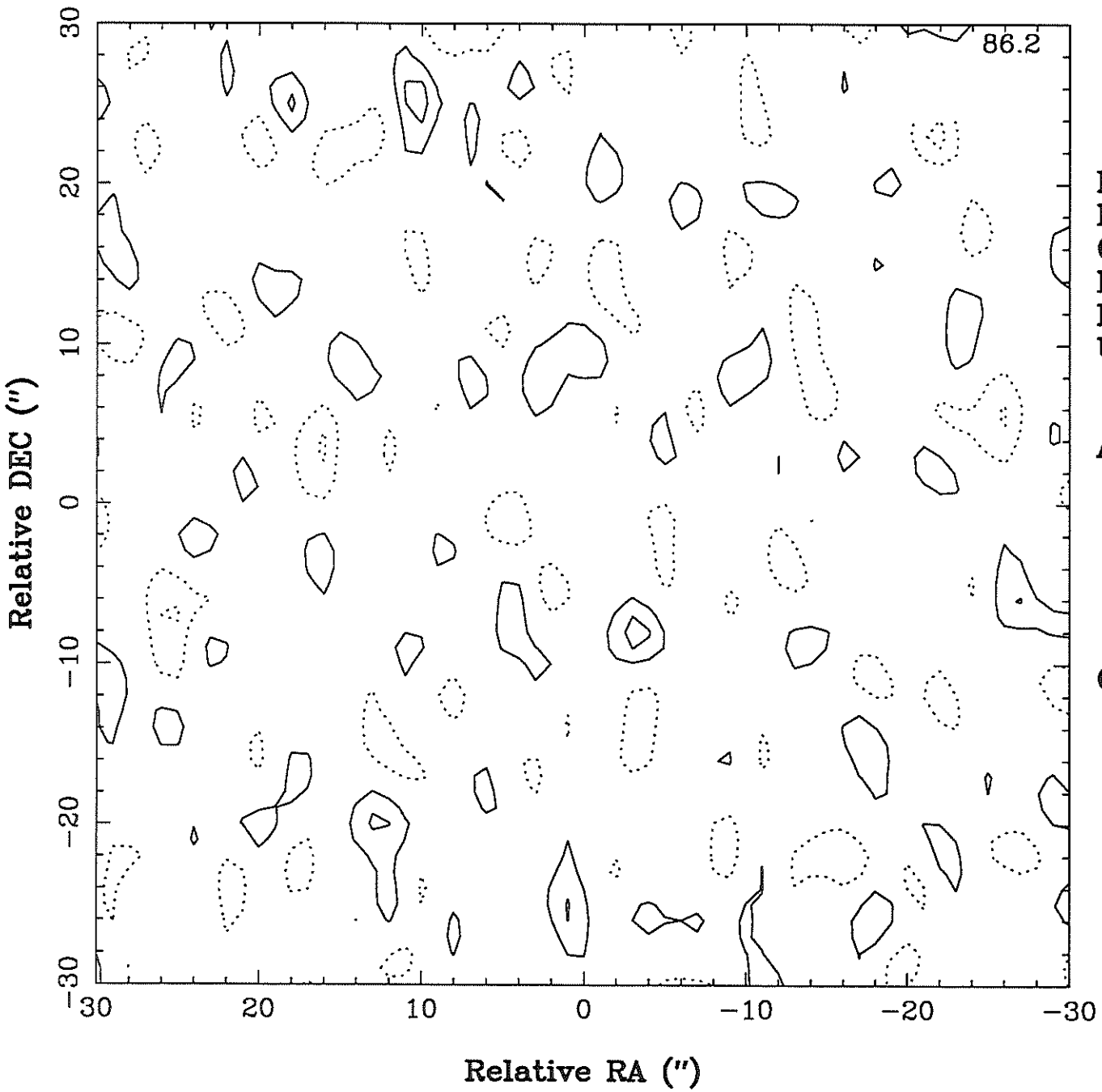

2005P403

20:05:59.56 40:21:01.80

File: rm
Freq: 0.000000 (GHz)
Crval3: 86.2020 GHz
Max: 0.122131
Min: −0.117029
Units: JY/BEAM

Axes: 64 x 64 x 1
−1.00 x 1.00 x 0.31

Contours: 10

0.050	0.100
0.200	0.300
0.400	0.500
0.600	0.700
0.800	0.900

(a) MOSAIC OF DECONVOLVED FIELDS

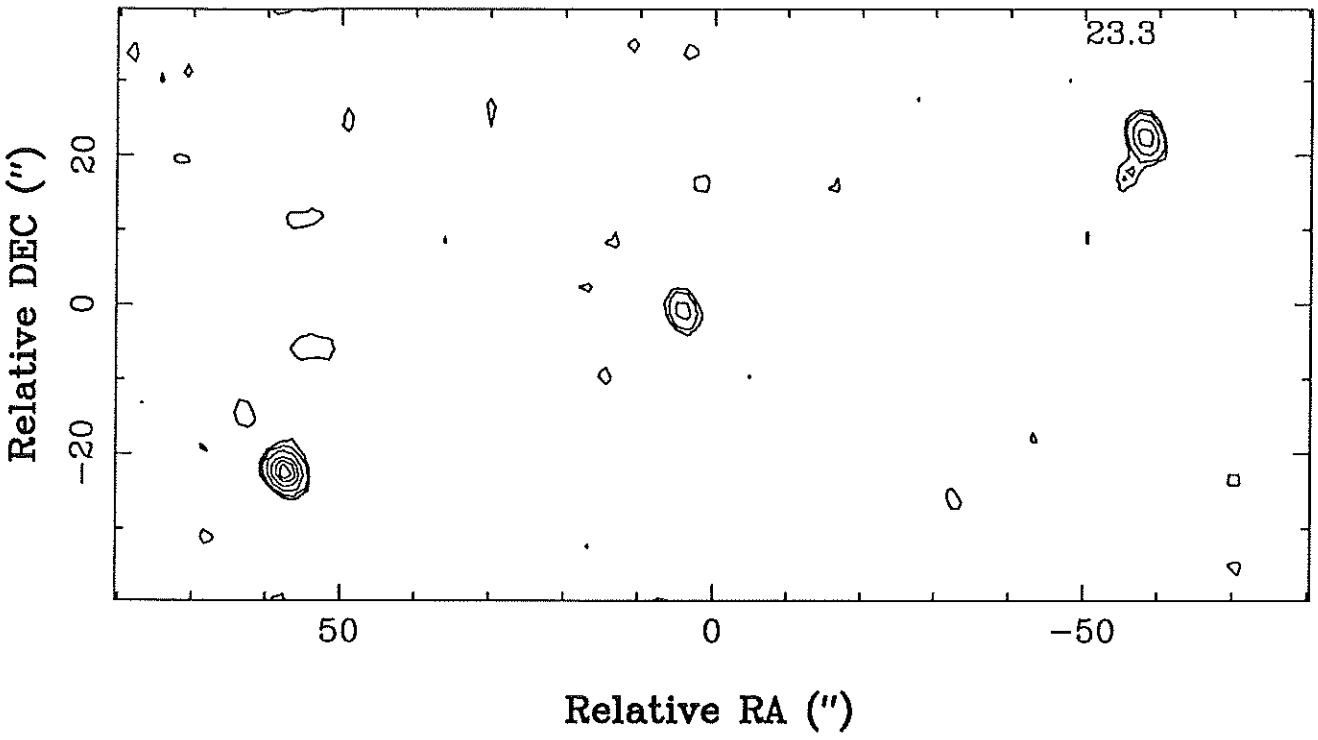

(b) MOSAIC AFTER AFTER SELF-CALIBRATION